RESEARCH ARTICLE

Check for updates

Sequential enhancement of proton conductivity by aliovalent cadmium substitution and post-synthetic esterolysis in a carboxylate-functionalized indium framework with dimethylaminium templates†

Hui Gao, ‡[a,b] Ying-Xia Wang, ‡[a] Yan-Bin He [b] and Xian-Ming Zhang *[a,c]

A sequential improvement strategy has been devised and implemented on a 3D open framework **In-BQ** showing 2D intersected channels filled by dimethylamine and its protonated cation constructed by $-COOCH_3-$functionalized anilicate linkers. *In situ* aliovalent metal substitution and post-synthetic ligand esterolysis led to **Cd-BQ-COOH** with a doubling of $Me_2NH_2^+$ carriers and a great number of residual $-COOH$ groups, resulting in maximum proton concentration and frequent jumping sites. As a result, the modified **Cd-BQ-COOH** exhibits a 300-fold enhanced value of proton conductivity compared with that of pristine **In-BQ**, reaching 6.06×10^{-2} S cm^{-1}. MD calculations reveal that the entire process of proton transportation in **Cd-BQ-COOH** is achieved by the vehicle mechanism.

Introduction

Solid-state proton conductors have attracted considerable attention for a wide variety of applications in hydrogen separation, water electrolysis, biological sensors and fuel cells,[1,2] which are currently focused on dramatically improving their proton conductivity and deeply illuminating their intrinsic conducting pathways.[3,4] Compared with other inorganic metal oxides or organic polymers,[5,6] metal–organic frameworks (MOFs) are studied and accepted as preferred candidates for next-generation conducting materials due to their ordered crystalline nature, high internal porosity and tunable modular functionality.[7–10] These unique characteristics are beneficial not only to acquire rich proton sources in a restricted volume to increase proton carrier concentration but also to create abundant hopping sites in a specific alignment to elevate the proton mobility.[11,12] Although most MOF materials show good prospects, it is still required to tactically fine-tune key structural components towards the precise design of high-level performance and long-term durability of proton conduction.[13–15]

For this purpose, two distinct strategies involving predesigned methods or post-synthetic modifications[16–19] have been proposed and implemented to draw multiple proton carriers into MOFs: (1) the introduction of protophilic groups ($-SO_3H$, $-PO_3H_2$, $-COOH$, $-OH$, *etc.*) on the backbones by retaining residual acidic groups or transforming the precursors into functional groups;[20,21] (2) the incorporation of protic entities (H_2SO_4, H_3PO_4, imidazole, triazole, ammonium cations, *etc.*) into the channels by balancing charged frameworks or exchanging guest molecules.[22,23] Particularly, there have been some recent synergistic highly proton-conducting materials originating from the aforementioned approaches, for example H_2SO_4@MIL-101-SO_3H,[24] BUT-8(Cr)A,[25] and PCMOF2$\frac{1}{2}$(Tz).[26] These reasonable and sequential modifications of the products afford maximum proton donor–acceptor and strong host–guest interactions to establish successive hydrogen-bond networks and efficient proton-transfer pathways, leading to conductivity values surpassing 10^{-1} S cm^{-1} below 373 K with humidification, which are comparable to that of commercial Nafion materials.[27–29]

Inspired by the feasibility of the above tactics, we attempt to explore enhancing strategies with synergistic effects to optimize proton conduction performance. In a previous report, we proposed an aliovalent metal substitution strategy[30,31] and implemented it on a dimethylaminium-tem-

[a]Key Laboratory of Magnetic Molecules and Magnetic Information Material of Ministry of Education, School of Chemistry and Material Science, Shanxi Normal University, Taiyuan, Shanxi, 030006, P. R China. E-mail: zhangxm@dns.sxnu.edu.cn, zhangxianming@tyut.edu.cn
[b]Department of Pharmacy, Changzhi Medical College, Changzhi, Shanxi, 046000, P. R. China
[c]College of Chemistry & Chemical Engineering, Key Laboratory of Interface Science and Engineering in Advanced Material, Ministry of Education, Taiyuan University of Technology, Taiyuan 030024, P. R. China

†Electronic supplementary information (ESI) available: Proton-conducting measurement, H_2O adsorption, IR, PXRD, TGA, MS, NMR data (PDF). ESI Videos of **Cd-BQ-COOH** and **In-BQ-COOH** are showing the proposed conduction mechanism (MP4). See DOI: https://doi.org/10.1039/d2qi00407k
‡These authors contribute equally to this work.

This journal is © the Partner Organisations 2022

Inorg. Chem. Front., 2022, **9**, 2997–3002 | **2997**

plated compound **In-BQ**.[31] This diamond-topology open framework featuring 2D intersected channels filled with dimethylamine and its protonated dimethylaminium constructed by –COOCH$_3$-functionalized anilicate linkers prompted us to sequentially modify the cooperation of aliovalent Cd(II) substitution and post-synthetic ligand esterolysis. Surprisingly, the modified framework **Cd-BQ-COOH** has three kinds of proton sources: the first are the attached –OH groups, which could dissociate H$^+$ during the coordinate progress; the second are the filled Me$_2$NH molecule and Me$_2$NH$_2^+$ cation, which could protonate into the doubling of Me$_2$NH$_2^+$ cations through the aliovalent replacement of In(III) by Cd(II); and the third are the functionalized –COOH groups, which are potentially converted from the post-synthetic esterolysis of –COOCH$_3$ on anilicate ligands. In contrast to the Cd(II)-substituted **Cd-BQ** and carboxyl-functionalized **In-BQ-COOH**, which have already boosted the proton conductivities by 100-fold (2.30×10^{-2} S cm^{-1}, 303 K and 95% RH) and 15-fold (3.54×10^{-3} S cm^{-1}, 303 K and 95% RH), respectively, when compared with pristine **In-BQ**, the sequentially modified **Cd-BQ-COOH** exhibits a 300-fold enhancement with up to 6.06×10^{-2} S cm^{-1} at the same condition.

Experimental section

Chemicals and materials

The starting materials and solvents were purchased and utilized from commercial sources without further purification. **In-BQ** and **Cd-BQ** were prepared according to our previously described procedure.[31] To maintain the integrity of the skeletons and reduce the possibility of losing molecules/cations in the pores as much as possible, a mild and reversible acid hydrolysis was employed. **In-BQ** (0.2 g) and **Cd-BQ** (0.2 g) were separately hydrolyzed with 1 M H$_2$SO$_4$ solution (20 mL) in a 50 mL round-bottom flask. The suspensions of the solid were stirred for 10 h at 40 °C. After cooling to about 30 °C, the resulting powdered solids were isolated by centrifugation and washed with H$_2$O several times until the upper fluid was neutral. The morphological changes in both materials before and after esterolysis are shown in Fig. S1.†

Physical characterization

Scanning electron microscopy (SEM) images were recorded using a Thermofisher APR 20 emission scanning electron microscope with an accelerating voltage of 2–10 kV. Powder X-ray diffraction (PXRD) was measured on a Rigaku D/max-2550 diffractometer using Cu Kα radiation with an angle range (2θ) from 5° to 50°. Fourier transform infrared spectra (FT-IR) were obtained on KBr pellets with a PERKIN-ELMER 100-IR spectrometer (400–4000 cm^{-1}) at 298 K. Thermal gravimetric analysis (TGA) curves were collected using a JUPITER STA 449F3 instrument in an air atmosphere with a heating rate of 10 °C min^{-1}. Nuclear magnetic resonance (NMR) data were analysed using a BRUKER AVANCE 400 spectrometer. Electrospray ionization-mass spectrometry (ESI-MS) was per-

formed on a BRUKER SolanX 70 FT-MS. The H$_2$O vapor adsorption isotherms were recorded using a BSD-VVS gravimetric vacuum steam adsorber at room temperature.

Proton conductivity measurement

The proton conductivity was tested using a Princeton ParStat-4000 electrochemical analyzer with a two-probe system at an AC voltage of 100 mV in the frequency range of 1 MHz to 0.1 Hz. The as-synthesized samples were pressed into pellets of 6.0 mm diameter and 1–2 mm thickness at a pressure of 20 MPa. The measured slice pellet was sandwiched between two stainless steel wafers and clamped with an electrode clip. The system temperature and humidity were controlled by a BLUEPARD BPS-50L programmable incubator. The proton conductivity (σ) was calculated according to eqn (1), where σ = proton conductivity (S cm^{-1}), L = the thickness (cm), A = surface area (cm^2), and R = impedance (Ω).

$$\sigma = \frac{L}{R \cdot A} \tag{1}$$

E_a is the activation energy, which was determined from the fitted slope of the Arrhenius eqn (2).

$$\sigma T = \sigma_o \exp\left(-\frac{E_a}{\kappa \cdot T}\right) \tag{2}$$

Computational details

The initial and fully hydrolyzed **In-BQ-COOH** and **Cd-BQ-COOH** structures were built and optimized on the basis of the **In-BQ** and **Cd-BQ** crystal structures, respectively. Subsequently, a computational unit involving a couple of Me$_2$NH$_2^+$ (or one Me$_2$NH$_2^+$ and one Me$_2$NH) and associated framework molecules was chosen as a theoretical model. The positions of the O atoms and C atoms of the framework were highly fixed to avoid crumbling or large structural distribution. Meanwhile, all atoms of H and the dimethylaminium templates remained free, allowing proton carriers with H$^+$ to perform transportation or exchange. The entire model was fixed in a simulation box with a vacuum area of 10 Å^3. The quantum molecular dynamics (MD) were simulated using the SIESTA package[32] with the GGA-PBE functional[33] and Troullier–Martins norm-conserving pseudopotentials.[34] A double-ζ polarized (DZP) basis set was employed for the valence electronic orbitals of all atoms and the mesh cut-off was set as 250 Ry. The Monkhorst–Pack type of k-point sampling with a ($1 \times 1 \times 1$) mesh was used for the **In-BQ-COOH** and **Cd-BQ-COOH** structure models. The MD simulation was controlled by the Nosé[35] method employing 2000 steps at a time step of 1 fs at 298 K.

Results and discussion

In the host backbone of **In-BQ**, each In(III) ion is eight-coordinated with O atoms belonging to four anilicate ligands in the chelate mode, and each linker is connected to two In(III)

2998 | *Inorg. Chem. Front.*, 2022, **9**, 2997–3002

This journal is © the Partner Organisations 2022

ions in a bis-bidentate fashion, building a 3D diamond-topology structure containing 2D intersected channels. The channels are decorated by coordinated –OH groups and residual –COOCH$_3$ groups, as well as filled with a Me$_2$NH molecule and a Me$_2$NH$_2^+$ counterion. Accompanied with the *in situ* aliovalent replacement of In(III) by Cd(II), the original Me$_2$NH/Me$_2$NH$_2^+$ in **In-BQ** protonate into the doubling of Me$_2$NH$_2^+$ cations in **Cd-BQ** for charge balance. Moreover, the absolute freedom of the –COOCH$_3$ groups on the anilicate linkers offers an uncommon opportunity for the –COOH ligand functionalization to confer this material with advanced proton conduction performance. Through the post-synthetic esterolysis of **In-BQ** and **Cd-BQ** by H$_2$SO$_4$ (1 M) aqueous solution, the modified frameworks have been generated, denoted as **Cd-BQ-COOH** and **In-BQ-COOH**, respectively (Fig. 1).

Notably, the hydrogen bonds in **Cd-BQ-COOH** [N–H⋯O (2.86–3.10 Å) and O–H⋯O (2.61–3.69 Å)] are much shorter than those in **In-BQ-COOH** [N–H⋯O (2.97–3.65 Å) and O–H⋯O (2.71 Å)] (Table S1† and Fig. 2), and are much richer than those in **Cd-BQ** and **In-BQ** as well (Fig. S2†). Apparently, the multi-step route of Cd(II) substitution and –COOH functionalized modification gives rise to an expanded hydrogen-bond network, and endows **Cd-BQ-COOH** with progressively boosted proton conductivity.
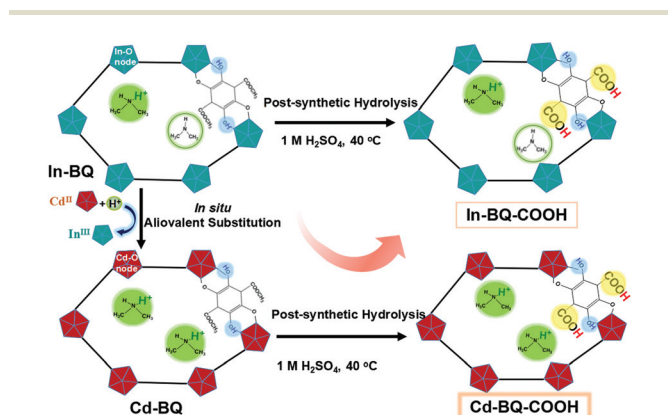

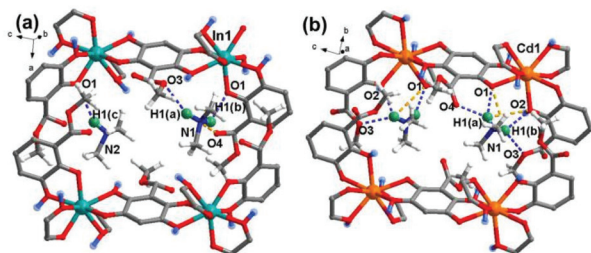**Fig. 1** The formation processes for **In-BQ-COOH** and **Cd-BQ-COOH**.

Fig. 2 Comparison of the H-bond arrangements of (a) **In-BQ-COOH** and (b) **Cd-BQ-COOH**. Note: The H atoms of –OH, –COOH, and Me$_2$NH/Me$_2$NH$_2^+$ are highlighted in blue, yellow, and green, respectively. The blue and orange dashed lines denote the N–H⋯O and O–H⋯O bonds, respectively.

The PXRD profiles before and after the proton-conducting tests of **In-BQ-COOH** and **Cd-BQ-COOH** are matched well with the simulated and as-synthesized patterns of the **In-BQ** and **Cd-BQ** frameworks, respectively, demonstrating the existence of the crystalline structures after the entire post-synthetic treatments and impedance measurements (Fig. S3†). Additionally, the –COOH functionalization frameworks were confirmed by FT-IR (Fig. S4†). The absorption peaks of the –COOCH$_3$ group located at 1720 and 1150 cm^{-1} in **In-BQ** and 1730 and 1300 cm^{-1} in **Cd-BQ**, respectively, are weakened in the spectra of **In-BQ-COOH** and **Cd-BQ-COOH**, and several peaks appear near 1710 and 900 cm^{-1} stemming from the C=O and O–H stretching vibrations, respectively. To further confirm the production of the –COOH group, we performed ESI-MS and NMR analyses (Fig. S5 and S6†). The ESI-MS spectrum after hydrolysis shows high intensity peaks at *m/z* values of 227.45 and 256.24, while the spectrum before hydrolysis only shows one intensity peak at 256.77. The new peak position fits well with the mass of the expected carboxylic fragment. In the ^{1}H-NMR spectra, where dibromide was used as a reference, the integral area of –CH$_3$ was obviously diminished after hydrolysis, indirectly demonstrating the formation of –COOH. Both frameworks after hydrolysis show almost identical proportion of losing weight from **In-BQ** and **Cd-BQ** at the first step in the range of 30–150 °C, suggesting that the guest molecules are retained without much damage (Fig. S7†). The different hydrophilicity of the inner pores has been characterized by H$_2$O vapor adsorption at 298 K (Fig. S8†). The H$_2$O vapor uptakes of **In-BQ-COOH** and **Cd-BQ-COOH** are 140 wt% and 102 wt%, respectively, much higher than the 58 wt% of **In-BQ** and 38 wt% of **Cd-BQ**.[31] This typical increase is associated with the effective transition of hydrophobic groups into hydrophilic groups hanging in the inner pore wall.

The proton-conductivities of **In-BQ-COOH** and **Cd-BQ-COOH** were measured by performing electrochemical impedance spectroscopy (EIS) on the pelletized powder samples. All resistance values were estimated from the *Z'* intercept values due to the imperfect semicircle of the Nyquist plots.[22,36] In order to evaluate the water affinities of these two compounds, under similar testing conditions to those of **In-BQ** and **Cd-BQ**, humidity-dependent proton conducting data were measured at 25 °C with RH increasing from 55% to 95% (Table S2 and Fig. S9†). At 55% RH, the conductive value of **Cd-BQ-COOH** is 4.85×10^{-6} S cm^{-1}, compared with the 8.27×10^{-6} S cm^{-1} of **In-BQ-COOH**. With rising humidity, the proton conductivity of **Cd-BQ-COOH** exceeds that of **In-BQ-COOH** and exhibits an ultrahigh conductive value of 3.03×10^{-2} S cm^{-1} at 95% RH, which is nearly 20 times higher than that of **In-BQ-COOH** (1.57×10^{-3} S cm^{-1}) at the same humidity. This increasing trend is consistent with the humidity-dependent results of **In-BQ** and **Cd-BQ**, and the proton conductivities are all improved under the parallel comparison. This is mainly attributed to the hydrophilicity of the –COOH groups, where absorbed water molecules acting as proton carriers could increase the efficiency of proton transfer.

This journal is © the Partner Organisations 2022

Inorg. Chem. Front., 2022, **9**, 2997–3002 | **2999**

To further investigate the potential conducting mechanism, the temperature-dependent proton conductivity, which is a key factor for the calculation of the resulting activation energy (E_a), was tested. Analogous to **Cd-BQ** and **In-BQ**, both **Cd-BQ-COOH** and **In-BQ-COOH** show better conductive behaviors in the low temperature region,[12,37,38] and thus the temperature-dependent conductive ability of these two compounds was characterized from 10 to 30 °C under 95% RH (Fig. 3, Fig. S10 and Table S3†). At 10 °C, the conducting values of **Cd-BQ-COOH** and **In-BQ-COOH** are 2.01×10^{-2} S cm^{-1} and 8.75×10^{-4} S cm^{-1}, respectively. As the temperature increases to 30 °C, the conductivities increase and reach their maximum values of 6.06×10^{-2} S cm^{-1} and 3.54×10^{-3} S cm^{-1}, respectively. The conductivities of **Cd-BQ-COOH** and **In-BQ-COOH** are also compared with other reported MOF-based proton conductors by ligand post-synthetic modification, as shown in Table S4.† Obviously, the 20-fold increased conductivities of the two compounds in the same range are almost maintained. As a comparison, the E_a values of **Cd-BQ-COOH** and **In-BQ-COOH** are determined using the Arrhenius equation and found to be 0.41 eV and 0.56 eV, respectively, much lower than the 0.48 eV of **Cd-BQ** and 0.73 eV of **In-BQ**.[31] This result suggests that the energy consumption of the proton transportation in both compounds decreases with the participation of the –COOH groups, and the intrinsic proton migration may be due to the vehicle mechanism.

MD calculation has been recognized as a promising method to clearly elucidate the proton transportation mechanism at the atomic scale.[39–43] Based on this, further simulation studies on **Cd-BQ-COOH** and **In-BQ-COOH** were performed by first-principles calculations with an assumption that all the ester groups in **Cd-BQ** and **In-BQ** were completely replaced by –COOH groups.

At the initial situation in **Cd-BQ-COOH** (Fig. 4a), the Me$_2$NH$_2^+$ cation mainly spins and glides around the Cd1(a)

Fig. 4 Migration trajectory of Me$_2$NH$_2^+$ in **Cd-BQ-COOH** at (a) the initial state; (b and c) the intermediate states; and (d) the later state. (e and f) The pathway of proton hopping between the –OH group and –COOH group in **In-BQ-COOH**. (g) A strong interaction is established between the H$^+$ and Me$_2$NH. (h) Formation of a protonated Me$_2$NH$_2^+$. Note: The Me$_2$NH/Me$_2$NH$_2^+$ and the hopping protons are highlighted in green. The blue and orange dashed lines illustrate the changes of N–H···O and O–H···O bonds, respectively.
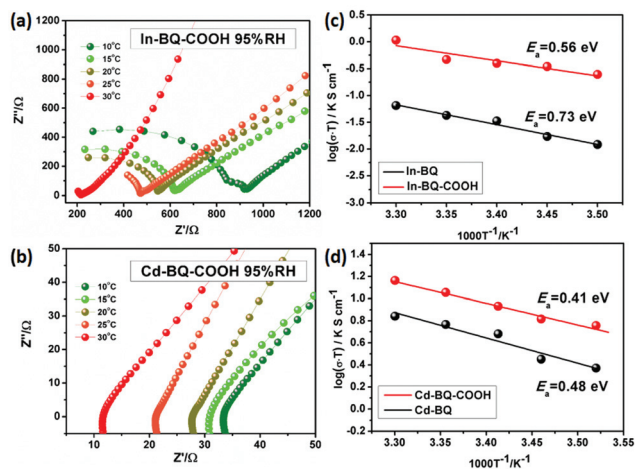

Fig. 3 Impedance spectra of (a) **In-BQ-COOH** and (b) **Cd-BQ-COOH** at 10−30 °C under 95% RH. Comparison of the Arrhenius plots of (c) **In-BQ-COOH** and (d) **Cd-BQ-COOH** with **In-BQ** and **Cd-BQ**, respectively, at 10−30 °C under 95% RH.
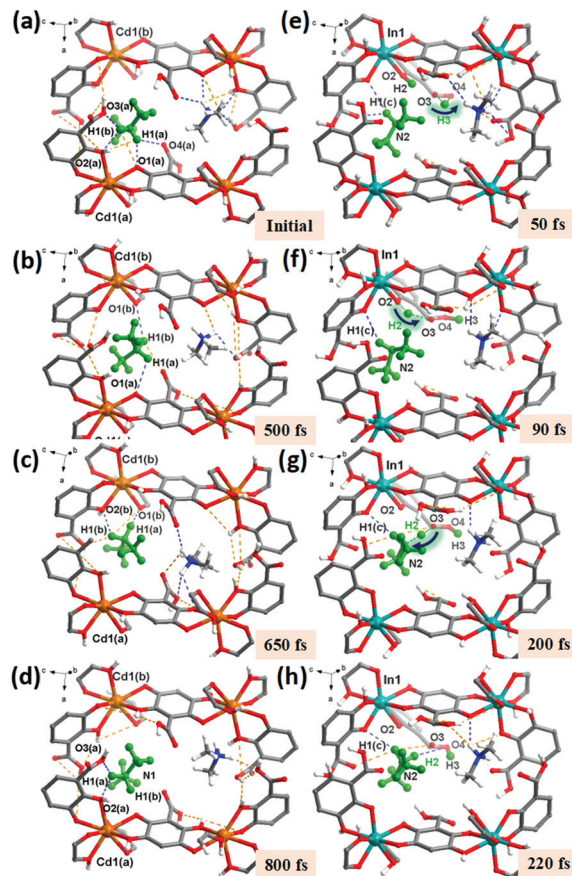
atom through the breakage and reestablishment of H-bonds. Then, at ~500 fs (Fig. 4b), the H1(a) and H1(b) atoms on the Me$_2$NH$_2^+$ cation keep on moving towards the central region of the channel, building almost equal lengths of H-bonds with O1(a) and O1(b). Accompanied by the continuous movement of the Me$_2$NH$_2^+$ cation at 650 fs, the H-bonds between H1(a) and H1(b) with O1(b) and O2(b) are re-established, as shown in Fig. 4c, which lead to the protons transferring near Cd1(b). In the final process (Fig. 4d), the Me$_2$NH$_2^+$ cation migrates and returns near Cd1(a) by means of the H-bonds established with O2(a) and O3(a). It can be clearly seen that in the whole progress of proton transmission, the Me$_2$NH$_2^+$ cation acts as a whole to undergo self-rotation and migration in the counter-clockwise direction of "Cd1(a)–Cd1(b)–Cd1(a)".

Besides, in **In-BQ-COOH**, an interesting consecutive proton reorientation occurs on the Me$_2$NH molecule and finally protonates the Me$_2$NH$_2^+$ cation. Fig. 4e represents the situation at 50 fs, where the H3 atom on the –COOH group jumps from the O3 atom to the O4 atom following the intramolecular H-bond.

Subsequently at ~90 fs, the O3 atom acting as a hopping site accepts the H2 atom coordinated with the O2 atom belonging to –OH moieties (Fig. 4f). This intermediate stage of the H2 proton on O3 is estimated to be ~100 fs. Then with the self-rotation and vibration of the Me_2NH molecule, the H2 atom jumps from the O3 atom to the N2 atom at 200 fs, which corresponds to an O···N distance of 2.58 Å and an O3–H2···N2 angle of 162(08)° (Fig. 4g). In the later process, the protonated $Me_2NH_2^+$ cation as a whole continues to migrate (Fig. 4h). Overall, the entire process of proton migration involves the moving sequence of "O2–O3–N2", which is jointly achieved by the hopping mechanism and the vehicle mechanism.

Conclusions

In summary, by sequentially realizing *in situ* aliovalent Cd(II) substitution and post-synthetic ligand esterolysis on a 3-D diamond-like open framework **In-BQ**, we have successfully acquired the modified framework **Cd-BQ-COOH**, which possesses the doubling of $Me_2NH_2^+$ proton carriers and a great number of residual –COOH groups. These proton sources and hopping sites are beneficial to establish abundant hydrogen-bond networks and strong host–guest interaction, which lead to a 300-fold enhanced conductivity compared with that of pristine **In-BQ**, reaching 6.06×10^{-2} S cm^{-1} at 303 K and 95% RH. This work not only confirms the effectiveness and feasibility of the aliovalent metal substitution strategy extended to ligand modification but also provides a promising route to maximize the proton conduction performance of MOF materials.

Author contributions

Hui Gao: Conceptualization, investigation, formal analysis, visualization, writing-original draft. Ying-Xia Wang: Investigation, formal analysis, writing-review & editing. Yan-Bin He: Conceptualization (computations), investigation (computations). Xian-Ming Zhang: Conceptualization, project administration, funding acquisition, supervision, writing-review & editing.

Conflicts of interest

The authors declare that they have no conflict of interest. The authors declare no competing financial interests.

Acknowledgements

Notes and references

1 K. D. Kreuer, S. J. Paddison, E. Spohr and M. Schuster, Transport in proton conductors for fuel-cell applications: simulations, elementary reactions, and phenomenology, *Chem. Rev.*, 2004, **104**, 4637–4678.

2 H. Zhang and P. K. Shen, Recent development of polymer electrolyte membranes for fuel cells, *Chem. Rev.*, 2012, **112**, 2780–2832.

3 X. Meng, H. N. Wang, S. Y. Song and H. J. Zhang, Proton-conducting crystalline porous materials, *Chem. Soc. Rev.*, 2017, **46**, 464–480.

4 A. Shigematsu, T. Yamada and H. Kitagawa, Wide control of proton conductivity in porous coordination polymers, *J. Am. Chem. Soc.*, 2011, **133**, 2034–2036.

5 E. A. Sanginov, K. S. Novikova, N. N. Dremova and Y. A. Dobrovolskii, Formation of proton-conducting polymer additives based on sulfonated crosslinked polystyrene in nafion membranes, *Polym. Chem.*, 2019, **61**, 98–107.

6 H. Y. Sun, S. H. Sun, B. Hu, L. K. Gong, Y. M. Zou, J. L. Li, M. L. Feng and X. Y. Huang, Anisotropic proton conduction realized by a layered vanadium selenite single crystal, *Inorg. Chem. Front.*, 2020, **7**, 1699–1703.

7 J. H. Wang, Y. Zhang, M. Li, S. Yan, D. Li and X. M. Zhang, Solvent-assisted metal metathesis: a highly efficient and versatile route towards synthetically demanding chromium metal-organic frameworks, *Angew. Chem., Int. Ed.*, 2017, **56**, 6478–6482.

8 R. X. Yao, H. H. Fu, B. Yu and X. M. Zhang, Chiral metal-organic frameworks constructed from four-fold helical chain SBUs for enantioselective recognition of α-hydroxy/amino acids, *Inorg. Chem. Front.*, 2018, **5**, 153–159.

9 X. Chen and G. Li, Proton conductive Zr-based MOFs, *Inorg. Chem. Front.*, 2020, **7**, 3765–3784.

10 Q. X. Wang and G. Li, Bi(III) MOFs: syntheses, structures and applications, *Inorg. Chem. Front.*, 2021, **8**, 572–589.

11 A. L. Li, Q. Gao, J. Xu and X. H. Bu, Proton-conductive metal-organic frameworks: recent advances and perspectives, *Coord. Chem. Rev.*, 2017, **344**, 54–82.

12 T. Panda, T. Kundu and R. Banerjee, Self-assembled one dimensional functionalized metal-organic nanotubes (MONTs) for proton conduction, *Chem. Commun.*, 2012, **48**, 5464–5466.

13 X. X. Xie, Y. C. Yang, B. H. Dou, Z. F. Li and G. Li, Proton conductive carboxylate-based metal–organic frameworks, *Coord. Chem. Rev.*, 2020, **403**, 2131001–2131031.

14 J. Jiang and O. M. Yaghi, Bronsted acidity in metal-organic frameworks, *Chem. Rev.*, 2015, **115**, 6966–6997.

15 S. Chand, S. M. Elahi, A. Pal and M. C. Das, Metal-organic frameworks and other crystalline materials for ultrahigh superprotonic conductivities of 10−2 S cm−1 or higher, *Chem*, 2019, **25**, 6259–6269.

16 S. J. Liu, C. Cao, F. Yang, M. H. Yu, S. L. Yao, T. F. Zheng, W. W. He, H. X. Zhao, T. L. Hu and X. H. Bu, High proton conduction in two CoII and MnII anionic metal–organic frameworks derived from 1,3,5-benzenetricarboxylic acid, *Cryst. Growth Des.*, 2016, **16**, 6776–6780.

This journal is © the Partner Organisations 2022

Inorg. Chem. Front., 2022, **9**, 2997–3002 | **3001**

17 S. Horike, D. Umeyama, M. Inukai, T. Itakura and S. Kitagawa, Coordination-network-based ionic plastic crystal for anhydrous proton conductivity, *J. Am. Chem. Soc.*, 2012, **134**, 7612–7615.

18 J. Taylor, M. Komatsu, T. Dekura, S. Otsubo, K. M. Takata and H. Kitagawa, The role of a three dimensionally ordered defect sublattice on the acidity of a sulfonated metal-organic framework, *J. Am. Chem. Soc.*, 2015, **137**, 11498–11506.

19 T. H. N. Lo, M. V. Nguyen and T. N. Tu, An anchoring strategy leads to enhanced proton conductivity in a new metal-organic framework, *Inorg. Chem. Front.*, 2017, **4**, 1509–1516.

20 W. J. Phang, H. Jo, W. R. Lee, J. H. Song, K. Yoo, B. S. Kim and C. S. Hong, Superprotonic conductivity of a UiO-66 framework functionalized with sulfonic acid groups by facile postsynthetic oxidation, *Angew. Chem.*, 2015, **127**, 5231–5235.

21 R. L. Liu, D. Y. Wang, J. R. Shi and G. Li, Proton conductive metal sulfonate frameworks, *Coord. Chem. Rev.*, 2021, **431**, 213747–213772.

22 H. B. Luo, Q. Ren, P. Wang, J. Zhang, L. Wang and X. M. Ren, High proton conductivity achieved by encapsulation of imidazole molecules into proton-conducting MOF-808, *ACS Appl. Mater. Interfaces*, 2019, **11**, 9164–9171.

23 V. G. Ponomareva, K. A. Kovalenko, A. P. Chupakhin, D. N. Dybtsev, E. S. Shutova and V. P. Fedin, Imparting high proton conductivity to a metal-organic framework material by controlled acid impregnation, *J. Am. Chem. Soc.*, 2012, **134**, 15640–15643.

24 X. M. Li, L. Z. Dong, S. L. Li, G. Xu, J. Liu, F. M. Zhang, L. S. Lu and Y. Q. Lan, Synergistic conductivity effect in a proton sources-coupled metal-organic framework, *ACS Energy Lett.*, 2017, **2**, 2313–2318.

25 F. Yang, G. Xu, Y. Dou, B. Wang, H. Zhang, H. Wu, W. Zhou, J. R. Li and B. Chen, A flexible metal-organic framework with a high density of sulfonic acid sites for proton conduction, *Nat. Energy*, 2017, **2**, 877–883.

26 S. Kim, B. Joarder, J. A. Hurd, J. Zhang, K. W. Dawson, B. S. Gelfand, N. E. Wong and G. K. H. Shimizu, Achieving superprotonic conduction in metal-organic frameworks through iterative design advances, *J. Am. Chem. Soc.*, 2018, **140**, 1077–1082.

27 D. W. Lim and H. Kitagawa, Rational strategies for proton-conductive metal-organic frameworks, *Chem. Soc. Rev.*, 2021, **50**, 6349–6368.

28 D. W. Lim and H. Kitagawa, Proton transport in metal-organic frameworks, *Chem. Rev.*, 2020, **120**, 8416–8467.

29 H. N. Wang, H. X. Sun, Y. M. Fu, X. Meng, Y. H. Zou, Y. O. He and R. G. Yang, Varied proton conductivity and photoreduction CO2 performance of isostructural heterometallic cluster based metal-organic frameworks, *Inorg. Chem. Front.*, 2021, **8**, 4062–4071.

30 H. Gao, Y. B. He, J. J. Hou and X. M. Zhang, In situ aliovalent nickle substitution and acidic modification of nanowalls promoted proton conductivity in a In-OF with 1-D helical channel, *ACS Appl. Mater. Interfaces*, 2021, **13**, 38289–38295.

31 H. Gao, Y. B. He, J. J. Hou, Q. G. Zhai and X. M. Zhang, Enhanced proton conductivity by aliovalent substitution of cadmium for indiumin dimethylaminium templated metal anilicates, *ACS Appl. Mater. Interfaces*, 2020, **12**, 41605–41612.

32 J. M. Soler, E. Artacho, J. D. Gale, A. García, J. Junquera, P. Ordejón and D. Sánchez-Portal, The siesta method for ab Initio order-N materials simulation, *J. Phys.: Condens. Matter.*, 2002, **14**, 2745–2779.

33 J. P. Perdew, K. Burke and M. Ernzerhof, Generalized gradient approximation made simple, *Phys. Rev. Lett.*, 1996, **77**, 3865–3868.

34 N. Troullier and J. L. Martins, Efficient pseudopotentials for plane-wave calculations, *Phys. Rev. B: Condens. Matter Mater. Phys.*, 1991, **43**, 1993–2006.

35 S. Nosé, A unified formulation of the constant temperature molecular dynamics methods, *J. Chem. Phys.*, 1984, **81**, 511–519.

36 D. Umeyama, S. Horike, M. Inukai, Y. Hijikata and S. Kitagawa, Confinement of mobile histamine in coordination nanochannels for fast proton transfer, *Angew. Chem., Int. Ed.*, 2011, **50**, 11706–11709.

37 T. Panda, T. Kundu and R. Banerjee, Structural isomerism leading to variable proton conductivity in Indium(III) isophthalic acid based frameworks, *Chem. Commun.*, 2013, **49**, 6197–6199.

38 L. F. Zou, S. Yao, J. Zhao, D. S. Li, G. H. Li, Q. S. Huo and Y. L. Liu, Enhancing proton conductivity in a 3D metal-organic framework by the cooperation of guest [Me2NH2]+ cations, water molecules, and host carboxylates, *Cryst. Growth Des.*, 2017, **17**, 3556–3561.

39 S. C. Pal, S. Chand, A. G. Kumar, P. G. M. Mileo, I. Silverwood, G. Maurin, S. Banerjee, S. M. Elahi and M. C. Das, , A Co(II)-coordination polymer for ultrahigh superprotonic conduction: an atomistic insight through molecular simulations and QENS experiments, *J. Mater. Chem. A*, 2020, **8**, 7847–7853.

40 M. Wahiduzzaman, S. Wang, J. Schnee, A. Vimont, V. Ortiz, P. G. Yot, R. Retoux, M. Daturi, J. S. Lee, J. S. Chang, C. Serre, G. Maurin and S. Devautour-Vinot, A high proton conductive hydrogen-sulfate decorated titanium carboxylate metal-organic framework, *ACS Sustainable Chem. Eng.*, 2019, **7**, 5776–5783.

41 D. W. Lim, M. Sadakiyo and H. Kitagawa, Proton transfer in hydrogen-bonded degenerate systems of water and ammonia in metal-organic frameworks, *Chem. Sci.*, 2019, **10**, 16–33.

42 E. Eisbein, J. O. Joswig and G. Seifert, Proton conduction in a mil-53(Al) metal-organic framework: confinement versus host/guest interaction, *J. Phys. Chem. C*, 2014, **118**, 13035–13041.

43 T. Grancha, J. Ferrando-Soria, J. Cano, P. Amorós, B. Seoane, J. Gascon, M. Bazaga-García, E. R. Losilla, A. Cabeza, D. Armentano and E. Pardo, Insights into the dynamics of grotthuss mechanism in a proton-conducting chiral Biomof, *Chem. Mater.*, 2016, **28**, 4608–4615.